Full Length Article

JHS(E)

Journal of Hand Surgery
(European Volume)
2019, Vol. 44(10) 1041–1048

DOI: 10.1177/1753193419876203
journals.sagepub.com/home/jhs


Quantitative three-dimensional assessment of Madelung deformity

Abbas Peymani[1,2], Johannes G. G. Dobbe[2], Geert J. Streekstra[2,3], Henry R. McCarroll[4] and Simon D. Strackee[1]

Abstract

In the diagnostic work-up of Madelung deformity conventional radiographic imaging is often used, assessing the three-dimensional deformity in a two-dimensional manner. A three-dimensional approach could expand our understanding of Madelung deformity's complex wrist anatomy, while removing inter- and intra-rater differences. We measured previous two-dimensional-based and newly developed three-dimensional-based parameters in 18 patients with Madelung deformity (28 wrists) and 35 healthy participants (56 wrists). Madelung deformity wrists have increased levels of ulnar tilt, lunate subsidence, lunate fossa angle, and palmar carpal displacement. The lunate fossa is more concave and irregular, and angles between scaphoid, lunate, and triquetral bones are decreased. These findings validate the underlying principles of current two-dimensional criteria and reveal previously unknown anatomical abnormalities by utilizing novel three-dimensional parameters to quantify the radiocarpal joint.

Keywords

Madelung deformity, wrist, wrist imaging, radiocarpal joint

Date received: 10th March 2019; revised: 14th August 2019; accepted: 25th August 2019

Introduction

Guillaume Dupuytren (1834) presented the first case of a rare wrist deformity. Otto Wilhelm Madelung (1878) was the first, however, to publish an in-depth analysis of the condition that later came to bear his name. Madelung deformity is an uncommon congenital deformity, characterized by volar subluxation of the hand, dislocation of the ulna, and ulnar and volar angulation of the distal radial epiphysis.

Various two-dimensional (2-D) radiographic criteria have been proposed for the diagnostic work-up, with the McCarroll criteria currently being the most used (McCarroll et al., 2005). These criteria are based on manual X-ray measurements, thereby introducing inter- and intra-rater differences and reducing the complex three-dimensional (3-D) anatomy to a 2-D view. This 2-D assessment has shown to be of limited diagnostic value (Farr et al., 2018; Tuder et al., 2008) and has prevented the quantification of several clinical features, including abnormalities of the lunate fossa and the proximal carpal row (Stehling et al., 2009). Nearly all previous studies have evaluated the deformity in 2-D form, with the majority adhering to the McCarroll criteria (Kampa et al., 2010; Laffosse et al., 2008; Mallard et al., 2013; Saffar and Badina, 2015; Steinman et al., 2013).

This study investigates the 3-D anatomy of Madelung deformity in 18 patients. The reusability of previous 2-D criteria is investigated and new 3-D parameters are developed. This automatic and objective approach could expand our understanding

[1]Department of Plastic, Reconstructive and Hand Surgery, University of Amsterdam, Amsterdam, Netherlands
[2]Department of Biomedical Engineering and Physics, University of Amsterdam, Amsterdam, Netherlands
[3]Department of Radiology and Nuclear Medicine, University of Amsterdam, Amsterdam, Netherlands
[4]Department of Orthopaedic Surgery, California Pacific Medical Center, San Francisco, CA, USA

Corresponding Author:
Abbas Peymani, Department of Plastic, Reconstructive and Hand Surgery, Amsterdam UMC, University of Amsterdam, Amsterdam Movement Sciences, Meibergdreef 9, Amsterdam, The Netherlands.
Email: a.peymani@amsterdamumc.nl

of Madelung deformity's complex anatomy, while removing inter- and intra-rater differences.

Methods

Study population

Patients with a diagnosis of Madelung deformity were identified by searching the electronic medical record database of our hospital, using the International Classification of Diseases, Ninth Revision, Clinical Modification (ICD-9-CM) code: 755.54. Patients that visited our medical centre between 2002 and 2018, for outpatient or inpatient care in our department, were identified. Patients were included if they had undergone CT scanning of at least one wrist prior to any surgical interventions. The accuracy of the ICD-9-CM codes was confirmed by reviewing medical notes of each patient; wrongly coded patients were excluded. In total, 18 patients were included, for which CT scans of 28 wrists were available. In addition, previously acquired CT scans of 56 wrists from 35 healthy participants (21 bilateral, 14 unilateral) were included to quantitatively investigate anatomical differences. None of the healthy participants had a medical history of disorders or a history of surgical interventions on the wrists.

Image segmentation and processing

CT scans were segmented using a custom-made software package (Dobbe et al., 2019), to acquire virtual 3-D models of the following wrist bones: radius, ulna, scaphoid, lunate, triquetrum, and capitate (Figure 1). These virtual models were exported and further processed using self-developed software programmed in MATLAB R2018b (MathWorks Inc., Natick, MA, USA). This software performs the following functions automatically: wrist alignment, detection of radial and ulnar landmarks, and calculation of multiple 3-D-based measurements.

Computation of 3-D measurements

The McCarroll criteria comprise four measurements: ulnar tilt, lunate subsidence, lunate fossa angle, and palmar carpal displacement (McCarroll et al., 2005). Based on the underlying concepts defined in the initial study, these measurements were translated for usage in a 3-D model. Next, several new parameters were developed based on previously described anatomical abnormalities, including dysplasia of the lunate fossa and the pyramidal configuration of the bones in the proximal carpal row (Cook et al., 1996; Harley et al., 2002; Kosowicz, 1962; Stehling et al., 2009). Scaphoid and lunate fossae were quantified through three parameters: articular surface area, concavity, and irregularity. To quantify the configuration of the proximal carpal row we calculated the angle between scaphoid, lunate, and triquetral bones. All calculations were done for Madelung deformity wrists ($n = 28$) and healthy wrists ($n = 56$). All measurement results were rounded to one decimal place.

Ulnar tilt measures the ulnar angulation of the distal radial articular surface on a postero-anterior (PA) wrist view. Ulnar tilt was calculated as 3-D by defining a vector connecting the centres of the scaphoid and lunate fossae, and subsequently recording the complement of the angle (defined as 90 minus the angle) in degrees between this vector and the longitudinal axis of the ulna (Figure 2(a)).

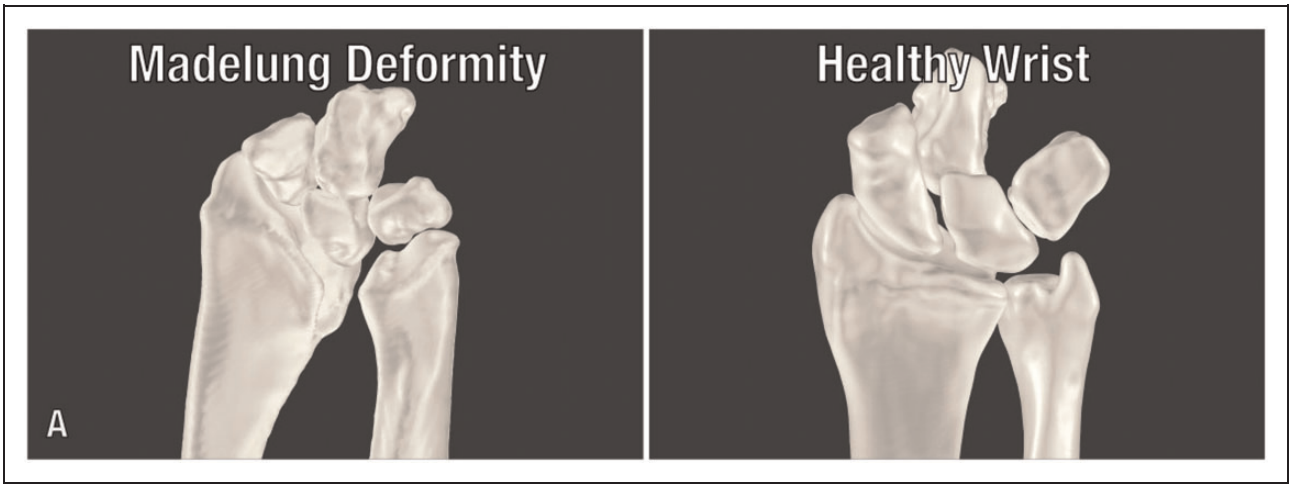

Figure 1. Three-dimensional reconstruction of wrist after segmentation of CT scan.

The analysis of scaphoid and lunate fossae is further described below. The longitudinal axis of the ulna was calculated by performing a principal component analysis on its virtual model, and recording the direction of maximal variance. *Lunate subsidence* measures the proximal displacement of the lunate bone (PA view). Lunate subsidence was calculated in our 3-D model by measuring the height difference between the ulnar styloid process and the base of the lunate bone (Figure 2(b)). The *Lunate fossa angle* measures the ulnar angulation of the lunate fossa (PA view). First, a 3-D plane was computed to fit the lunate fossa, using a least-squares fitting procedure. The lunate fossa angle was calculated by recording the complement of the angle in degrees, between the planes' normal vector and the longitudinal axis of the ulna (Figure 2(c)). *Palmar carpal displacement* measures the palmar-directed displacement of the carpus (represented by the lunate and capitate) relative to the longitudinal axis of the ulna (lateral view). To simulate a lateral wrist view, a 3-D plane was computed through the longitudinal axis of the ulna and the radial styloid process. Next, we calculated two vectors: one perpendicular vector from the plane to the most palmar point on the capitate, and one perpendicular vector from the plane to the most palmar point on the lunate. The length in millimetres of the longest vector was defined as the palmar carpal displacement (Figure 2(d)).

The articular surface areas of the scaphoid and lunate fossae were calculated in square millimetres (Figure 3(a)), using a method previously developed by the authors (Foumani et al., 2013; Peymani et al., 2017). The fossa concavity was calculated by fitting a sphere to its surface area, using a least-squares fitting procedure (Figure 3(b)). The inverse (1/R) of the sphere's radius in centimetres (R) defined the concavity of the fossa; higher value indicating a more concave (i.e. inwardly curved) shape of the fossa. Fossa irregularity was defined as the deviation of points on the articular surface area relative to the computed sphere; higher value indicating a more irregular (i.e. bumpy) surface area of the fossa (Figure 3(c)). Scapholunotriquetral (SLT) angle was calculated by recording the angle in degrees between two vectors: one vector from the centroid of the lunate bone to the centroid of the scaphoid bone, and one vector from the centroid of the lunate bone to the centroid of the triquetral bone (Figure 3(d)).

Statistical analysis

The following 3-D-based variables were used in statistical analyses: ulnar tilt, lunate subsidence, lunate fossa angle, palmar carpal displacement, articular surface area of the scaphoid/lunate fossae, concavity of the scaphoid/lunate fossae, irregularity of the scaphoid/lunate fossae, and SLT angle. To investigate differences between Madelung deformity wrists and healthy wrists, we compared the means of both groups. If a variable was normally distributed in both groups, an independent samples *t*-test (variances equal) or Welch's *t*-test (variances not equal) was performed. Equality of variances was assessed using Levene's test. If a variable was not normally distributed, the Mann–Whitney *U* test was performed. To control for possible confounding effects of age, binary logistic regression models were developed for each of our statistical analyses.

Results

Madelung deformity patients ($n = 18$) had a mean age of 21 years (SD 10) and all were women. Of these patients, 15 had a bilateral deformity (four confirmed genetic causes) and three had a unilateral deformity. Healthy participants ($n = 35$) had a mean age of 24 years (SD 6) and 24 were women.

There were significant differences in all 3-D-based parameters based on McCarroll criteria, between wrists of Madelung deformity patients and wrists of healthy participants (Table 1). After adjusting for age and excluding male participants from the healthy wrists, wrists of patients showed significantly increased levels of ulnar tilt, lunate subsidence, lunate fossa angle, and palmar carpal displacement.

For the newly developed 3-D-based wrist parameters (Table 2), significant age- and gender-adjusted differences were found between Madelung deformity wrists and healthy wrists. In patients' wrists, the articular surface areas of the scaphoid and lunate fossae were smaller, the lunate fossa was more concavely shaped, and the articular surface area of the lunate fossa was more irregular. Compared with healthy wrists, the proximal carpal row of Madelung deformity wrists showed a significantly increased SLT angle. No significant differences were found for concavity or irregularity of the scaphoid fossa.

Discussion

Our present study quantitatively assessed Madelung deformity in 3-D form and confirms that Madelung wrists have increased levels of ulnar tilt, lunate subsidence, lunate fossa angle, and palmar carpal displacement. The lunate fossa is more concave and irregular, and angles between scaphoid, lunate, and triquetral bones are decreased. A strength of this approach is that measurements are calculated

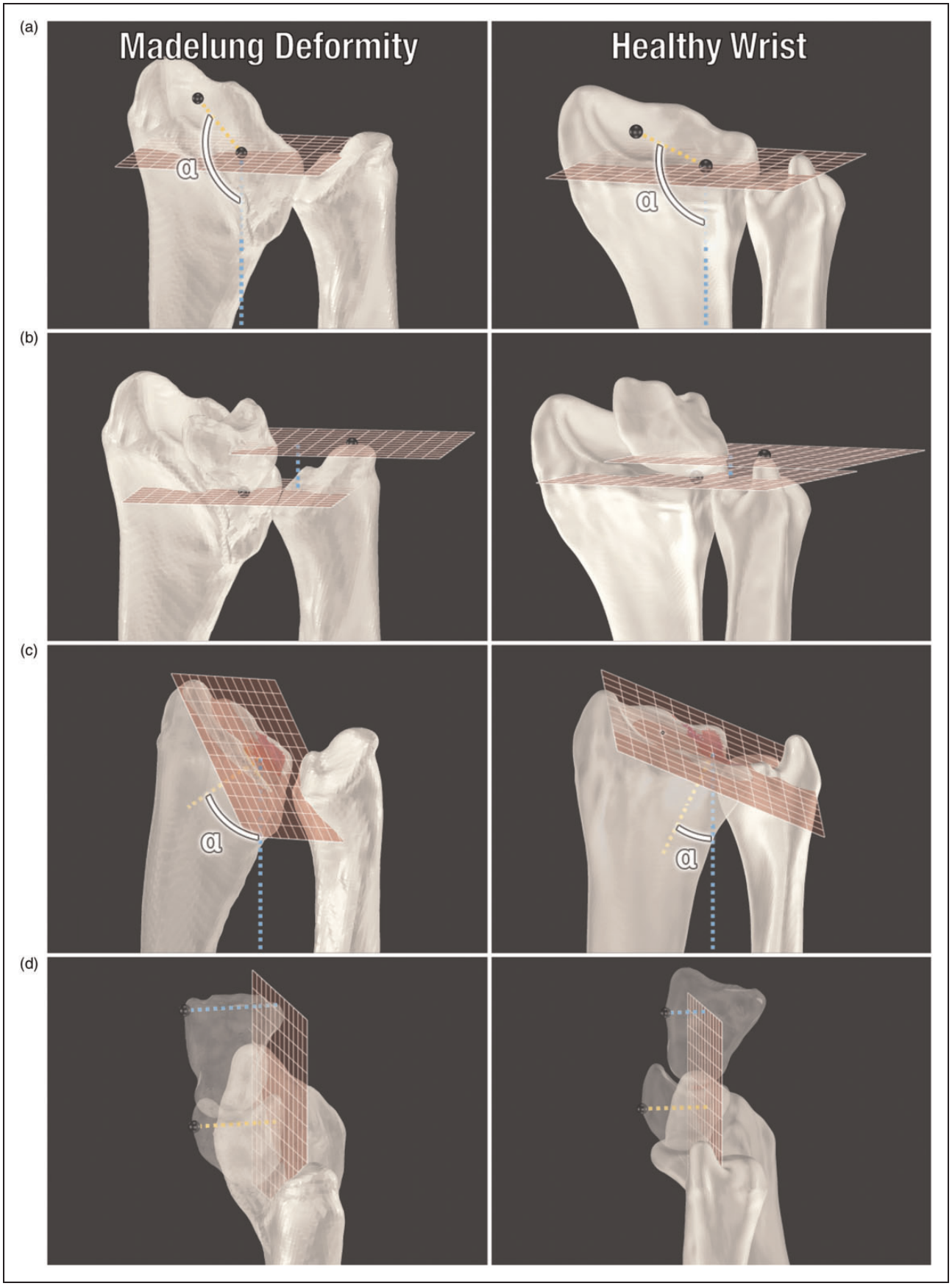

Figure 2. Visualization of 3-D wrist calculations based on the McCarroll criteria: (a) ulnar tilt; (b) lunate subsidence; (c) lunate fossa angle; (d) palmar carpal displacement.

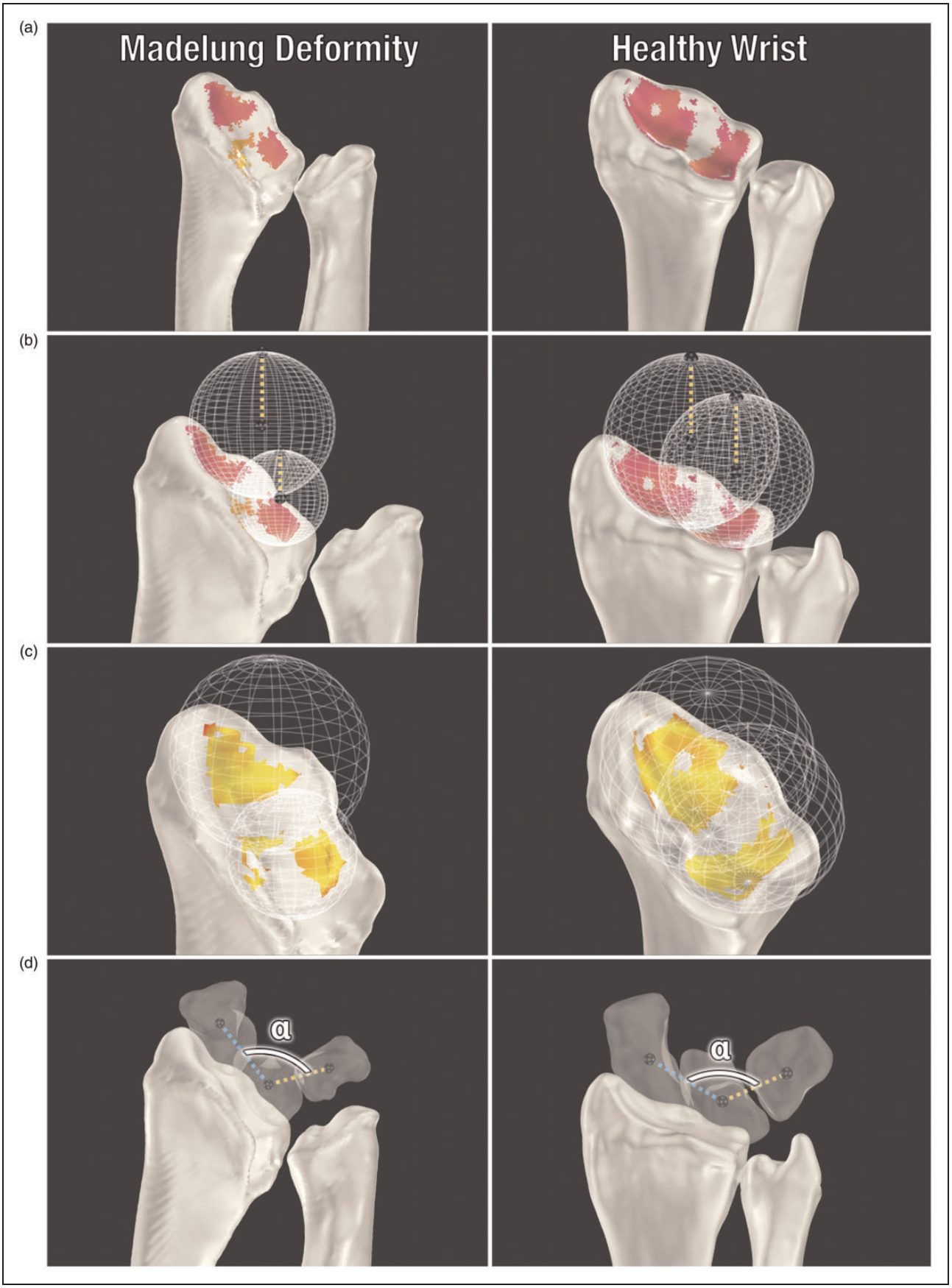

Figure 3. Visualization of novel 3-D wrist calculations: (a) articular surface areas of the scaphoid and lunate fossae; (b) concavity of the scaphoid and lunate fossae; (c) irregularity of the scaphoid and lunate fossae; (d) scapholunotriquetral angle.

Table 1. Three-dimensional-based wrist parameters based on McCarroll's criteria.

Parameters	Madelung deformity ($n=28$)	Healthy wrists ($n=56$)	p-value	p-value[a]
Ulnar tilt, degrees (SD)	37 (7.3)	23 (3.4)	<0.001	0.001
Lunate subsidence, mm (SD)	8.7 (4.0)	1.8 (2.2)	<0.001	<0.001
Lunate fossa angle, degrees (SD)	52 (13)	25 (4.0)	<0.001	0.005
Palmar carpal displacement, mm (SD)	16 (7.7)	13 (1.7)	0.001	0.014

[a]Adjusted for age and gender.

Table 2. Novel three-dimensional-based wrist parameters.

Parameters	Madelung deformity ($n=28$)	Healthy wrists ($n=56$)	p-value	p-value[a]
Scaphoid fossa surface area, mm^2 (SD)	77 (32)	130 (30)	<0.001	<0.001
Lunate fossa surface area, mm^2 (SD)	70 (25)	103 (26)	<0.001	0.009
Scaphoid fossa concavity, cm^{-1} (SD)	0.8 (0.1)	0.7 (0.1)	0.003	0.074
Lunate fossa concavity, cm^{-1} (SD)	0.9 (0.2)	0.8 (0.1)	<0.001	0.005
Scaphoid fossa irregularity, mm (SD)	0.2 (0.1)	0.2 (0.1)	0.178	0.789
Lunate fossa irregularity, mm (SD)	0.3 (0.1)	0.2 (0.1)	<0.001	<0.001
SLT angle, degrees (SD)	115 (7)	122 (5)	<0.001	0.002

[a]Adjusted for age and gender.

automatically, using self-developed algorithms that could find easy implementations in third-party software. Additionally, automatic analyses remove inter- and intra-rater differences, likely increasing data quality. The only manual step is the segmentation process, which is expected to have a negligible impact. The small number of patients is a limitation, although we included considerably more wrists ($n=28$) than patients ($n=18$) due to the high bilateral occurrence. Lastly, only a subset of our patients underwent corrective surgery and their outcomes were not reported in a homogenous manner; this precluded any discussion about the association between 3-D parameters and outcomes.

The McCarroll criteria are used to identify Madelung deformity and to monitor changes (McCarroll et al., 2010). However, measurements show differences both within and between raters (McCarroll et al., 2005). Also, despite previously established thresholds, considerable overlap with healthy wrists exists (McCarroll et al., 2008, 2010). Hegazy et al. (2019) recently developed a modified 2-D technique using the capitate as a bony landmark instead of the ulna, observing an improved inter-and intra-rater agreement for some, but not all measurements. While our automatic approach solves this issue, the overlap with healthy wrists was also evident in our study, giving rise to the question whether three-dimension holds any diagnostic advantages over two-dimension. Even if automatic 3-D measurements could decrease overlap due to their objective nature, both methods should be further investigated in regards to diagnostic efficacy. Nonetheless, our findings validate the underlying principles of previous McCarroll criteria, with significant differences being visible in 3-D assessments.

In the normal wrist, the distal radial articular surface is concave in both sagittal and coronal planes, containing the triangular-shaped scaphoid fossa and the quadrangular-shaped lunate fossa. Whereas patients' lunate fossa angles have been widely reported (McCarroll et al., 2010; Tuder et al., 2008; Zebala et al., 2007), the fossa shape has not been investigated. The abnormal lunate fossa shape in Madelung deformity is not surprising, as the deformity's pathogenesis involves a premature growth plate arrest at the volar/ulnar aspects of the distal radius (Ghatan and Hanel, 2013), while leaving the anatomy at the radial aspect relatively intact.

The proximal carpal bones have been reported to be pyramiding (Harley et al., 2002; Stehling et al., 2009), angular-shaped (Kosowicz, 1962), or V-shaped (Henry and Thorburn, 1967) rather than smoothly convex (Gilula, 1979). Kosowicz (1962)

quantified a so-called 'carpal angle' on 2-D radiographs of healthy participants (132°, SD 7.2°) and gonadal dysgenesis patients (118°, SD 6.6°). Instead, we quantified the proximal carpal row in Madelung deformity using a 3-D approach. Interestingly, Madelung deformity has been strongly associated with Turner syndrome, one of the causes of gonadal dysgenesis (Zhong and Layman, 2012), and we found comparable decreases.

Currently, most surgeons treat the deformity with osteotomies of the radius and/or ulna, the rationale being that restoring skeletal angles improves wrist biomechanics and function (dos Reis et al., 1998). Although postoperative outcomes seem satisfactory, some patients require revision surgery due to complications (Peymani et al., 2018). To advance our understanding of the anatomy and clinical outcomes of Madelung deformity, it is important to expand our scope beyond the traditional toolkit. In this study, we developed new parameters to quantify the radiocarpal joint. It is not unthinkable that a 'too abnormal' fossa concavity would indicate anatomical mismatching of the radiocarpal joint. Likewise, fossa irregularities could prognosticate joint degeneration. The aforementioned examples might inspire the surgeon to consider alternative treatment options in certain patients. Since there are still no evidence-based guidelines for corrective surgery in Madelung deformity (Peymani et al., 2018), improving existing and introducing new ways of wrist quantification might prove valuable in future prognostic models. However, further prospective studies are necessary to identify any association between these parameters and postoperative outcomes.

All our measurements were calculated using static CT scans. It would be beneficial to perform these calculations using dynamic four-dimensional imaging (Peymani et al., 2017). In addition to increasing the accuracy of fossae measurements by covering wrist bone positions during a patients' entire range of motion, it would reveal potential differences in carpal motion (Dobbe et al., 2019). The scope of this study was limited to the skeletal deformities, yet it may also be useful to investigate soft-tissue anomalies, including Vickers ligament (Steinman et al., 2013; Vickers and Nielsen, 1992) and the radiotriquetral ligament (Ali et al., 2015; Hanson et al., 2019), as the interplay between skeletal and ligamentous abnormalities is still unclear.

In summary, a 3-D approach to Madelung deformity validates the underlying principles of current 2-D criteria, and reveals previously unknown anatomical abnormalities by utilizing novel 3-D parameters to quantify the radiocarpal joint.

Declaration of conflicting interests The authors declared no potential conflicts of interest with respect to the research, authorship, and/or publication of this article.

Ethical approval This study was approved by the Medical Ethics Committee (NL66957.018.18) of the Amsterdam University Medical Center.

Funding The authors disclosed receipt of the following financial support for the research, authorship, and/or publication of this article: The first author (A.P.) received a PhD scholarship (2017) from the Amsterdam University Medical Center (Location AMC, Amsterdam, The Netherlands) supporting this research.

References

Ali S, Kaplan S, Kaufman T, Fenerty S, Kozin S, Zlotolow DA. Madelung deformity and Madelung-type deformities: a review of the clinical and radiological characteristics. Pediatr Radiol. 2015, 45: 1856–63.

Cook PA, Yu JS, Wiand W et al. Madelung deformity in skeletally immature patients: morphologic assessment using radiography, CT, and MRI. J Comput Assist Tomogr. 1996, 20: 505–11.

Dobbe JGG, de Roo MGA, Visschers JC, Strackee SD, Streekstra GJ. Evaluation of a quantitative method for carpal motion analysis using clinical 3-D and 4-D CT protocols. IEEE Trans Med Imaging. 2019, 38: 1048–57.

dos Reis FB, Katchburian MV, Faloppa F, Albertoni WM, Laredo Filho J Jr. Osteotomy of the radius and ulna for the Madelung deformity. J Bone Joint Surg Br. 1998, 80: 817–24.

Dupuytren G. *Leçons orales de clinique chirurgicale: Faites à l'hôtel-dieu de paris*. Chez Germer Baillière, 1834.

Farr S, Guitton TG, Ring D Science of Variation G. How reliable is the radiographic diagnosis of mild Madelung deformity? J Wrist Surg. 2018, 7: 227–31.

Foumani M, Strackee SD, van de Giessen M, Jonges R, Blankevoort L, Streekstra GJ. In-vivo dynamic and static three-dimensional joint space distance maps for assessment of cartilage thickness in the radiocarpal joint. Clin Biomech (Bristol, Avon). 2013, 28: 151–6.

Ghatan AC, Hanel DP. Madelung deformity. J Am Acad Orthop Surg. 2013, 21: 372–82.

Gilula LA. Carpal injuries: analytic approach and case exercises. AJR Am J Roentgenol. 1979, 133: 503–17.

Hanson TJ, Murthy NS, Shin AY, Kakar S, Collins MS. MRI appearance of the anomalous volar radiotriquetral ligament in true Madelung deformity. Skeletal Radiol. 2019, 48: 915–8.

Harley BJ, Carter PR, Ezaki M. Volar surgical correction of Madelung's deformity. Tech Hand Up Extrem Surg. 2002, 6: 30–5.

Hegazy G, Mansour T, Alshal E, Abdelaziz M, Alnahas M, El-Sebaey I. Madelung's deformity: capitate-related versus ulna-related measurement methods. J Hand Surg Eur. 2019, 44: 524–31.

Henry A, Thorburn MJ. Madelung's deformity. A clinical and cytogenetic study. J Bone Joint Surg Br. 1967, 49: 66–73.

Kampa R, Al-Beer A, Axelrod T. Madelung's deformity: radial opening wedge osteotomy and modified Darrach procedure using the ulnar head as trapezoidal bone graft. J Hand Surg Eur. 2010, 35: 708–14.

Kosowicz J. The carpal sign in gonadal dysgenesis. J Clin Endocrinol Metab. 1962, 22: 949–52.

Laffosse JM, Abid A, Accadbled F, Knor G, Sales de Gauzy J, Cahuzac JP. Surgical correction of Madelung's deformity by combined corrective radioulnar osteotomy: 14 cases with four-year minimum follow-up. Int Orthop. 2008, 33: 1655–61.

Madelung O. Die spontane subluxation der hand nach vorne. Verh Dtsch Ges Chir. 1878, 7: 259–76.

Mallard F, Jeudy J, Rabarin F et al. Reverse wedge osteotomy of the distal radius in Madelung's deformity. Orthop Traumatol Surg Res. 2013, 99: S279–83.

McCarroll HR, James MA, Newmeyer WL 3rd, Manske PR. Madelung's deformity: quantitative radiographic comparison with normal wrists. J Hand Surg Eur. 2008, 33: 632–5.

McCarroll HR Jr, James MA, Newmeyer WL 3rd, Manske PR. Madelung's deformity: diagnostic thresholds of radiographic measurements. J Hand Surg Am. 2010, 35: 807–12.

McCarroll HR Jr, James MA, Newmeyer WL 3rd, Molitor F, Manske PR. Madelung's deformity: quantitative assessment of x-ray deformity. J Hand Surg Am. 2005, 30: 1211–20.

Peymani A, Foumani M, Dobbe JGG, Strackee SD, Streekstra GJ. Four-dimensional rotational radiographic scanning of the wrist in patients after proximal row carpectomy. J Hand Surg Eur. 2017, 42: 846–51.

Peymani A, Johnson AR, Dowlatshahi AS et al. Surgical management of Madelung deformity: a systematic review. Hand. Epub ahead of print 13 August 2018. DOI: 10.1177/1558944718793179.

Saffar P, Badina A. Treatment of Madelung's deformity. Chir Main. 2015, 34: 279–85.

Stehling C, Langer M, Nassenstein I, Bachmann R, Heindel W, Vieth V. High resolution 3.0 tesla MR imaging findings in patients with bilateral Madelung's deformity. Surg Radiol Anat. 2009, 31: 551–7.

Steinman S, Oishi S, Mills J, Bush P, Wheeler L, Ezaki M. Volar ligament release and distal radial dome osteotomy for the correction of Madelung deformity: long-term follow-up. J Bone Joint Surg Am. 2013, 95: 1198–204.

Tuder D, Frome B, Green DP. Radiographic spectrum of severity in Madelung's deformity. J Hand Surg Am. 2008, 33: 900–4.

Vickers D, Nielsen G. Madelung deformity: surgical prophylaxis (physiolysis) during the late growth period by resection of the dyschondrosteosis lesion. J Hand Surg Br. 1992, 17: 401–7.

Zebala LP, Manske PR, Goldfarb CA. Madelung's deformity: a spectrum of presentation. J Hand Surg Am. 2007, 32: 1393–401.

Zhong Q, Layman LC. Genetic considerations in the patient with Turner syndrome—45,X with or without mosaicism. Fertil Steril. 2012, 98: 775–9.